Optical study of strained ultrathin films of strongly correlated LaNiO_{3}

M. K. Stewart, C.-H. Yee, Jian Liu, M. Kareev, R. K. Smith, B. C. Chapler, M. Varela, P. J. Ryan, K. Haule, J. Chakhalian, and D. N. Basov

Phys. Rev. B **83**, 075125 — Published 28 February 2011

DOI: 10.1103/PhysRevB.83.075125

Optical study of strained ultrathin films of strongly correlated $LaNiO_3$

M. K. Stewart,[1,*] C.- H. Yee,[2] Jian Liu,[3] M. Kareev,[3] R. K. Smith,[1] B. C. Chapler,[1] M. Varela,[4] P. J. Ryan,[5] K. Haule,[2] J. Chakhalian,[3] and D. N. Basov[1]

[1]*Department of Physics, University of California-San Diego, La Jolla, California 92093, USA*
[2]*Department of Physics & Astronomy, Rutgers University, Piscataway, New Jersey 08854-8019, USA*
[3]*Department of Physics, University of Arkansas, Fayetteville, Arkansas 72701, USA*
[4]*Materials Science & Technology Division, Oak Ridge National Laboratory, Oak Ridge, Tennessee 37831, USA*
[5]*X-Ray Science Division, Argonne National Laboratory, Argonne, Illinois 60439, USA*

(Dated: January 12, 2011)

An optical study of fully strained ultrathin $LaNiO_3$ films is presented and compared with LDA+DMFT calculations. $LaNiO_3$ films were grown by pulsed laser deposition on $LaAlO_3$ and $SrTiO_3$ substrates which provide compressive and tensile strain, respectively. Optical conductivity data show a Drude peak with a spectral weight that is significantly reduced compared to that obtained from LDA calculations. The extended Drude analysis reveals the presence of a pseudogap around 80 meV for the film on $SrTiO_3$ and near 40 meV, at low temperature only, for the film on LAO. An unusual temperature dependence of the optical conductivity is observed, with the Drude plasma frequency increasing by up to 20% at low temperature due to spectral weight transfer from bands lying 2-4 eV below the Fermi energy. Such a strong temperature dependence of the Drude spectral weight has previously been reported for correlated electron systems in which a phase transition is present. In LNO however, no phase transition is observed.

PACS numbers: 71.27.+a, 78.20.-e, 78.30.-j, 72.80.Ga

I. INTRODUCTION

Optical studies have been invaluable in the understanding of correlated electron systems, in part due to the optical sum rules which allow one to monitor redistributions of the electronic spectral weight associated with mobile and localized electrons.[1–3] One optical signature of correlations is especially notorious. The emergence of the conducting state in a correlated metal is usually associated with a dramatic transfer of the electronic spectral weight (SW) over many eV.[4–7] A canonical manifestation of this trend is seen in V_2O_3 as this correlated oxide undergoes an insulator-to-metal transition (IMT). Specifically, in V_2O_3 one registers a SW transfer from the energy range dominated by the response of the Hubbard bands to the quasiparticle peak responsible for the Drude response in the metallic state, confirming the validity of the half-filled Hubbard model.[4,8,9] Because the IMT in this and in other correlated systems is accompanied by structural changes and/or electronic/magnetic phase separation, the role of these auxiliary factors in the SW transfer is difficult to disentangle from the direct impact of correlations.

In this work, we present an optical study of $LaNiO_3$ (LNO), a correlated oxide[10–13] without additional complications due to phase transitions, spin or charge order, etc. This material is the only rare earth nickelate to remain metallic at all temperatures[14] and therefore offers the opportunity to study the dynamics of correlated electrons in its pure form, unobscured by structural or phase separation effects. The optical response of bulk LNO is unusual for a metal, showing no well defined Drude peak.[13,15] While the ultrathin strained films discussed here do exhibit a Drude resonance, electronic correlations dominate every aspect of charge dynamics. We show that the seemingly conventional metallic temperature dependence of the DC resistivity in LNO is directly linked to the unexpected enhancement of the Drude SW at the expense of features attributable to Mott-Hubbard bands.

II. METHODS

Epitaxial LNO films were grown by reflection high-energy electron diffraction (RHEED) controlled pulsed laser deposition on LAO and STO substrates with -1.2% and +1.7% lattice mismatch, respectively. The films are 30 unit cells thick with c-axis parameters of 3.86 Å on LAO and 3.78 Å on STO (see Table I). Representative time-dependent RHEED specular intensity (RSI) is shown in Fig.1 for the LNO film on STO. A full recovery of RSI is observed after each unit-cell layer, characteristic of perfect layer-by-layer growth. The inset in Fig.1 shows the corresponding RHEED image with well defined spots and streaks at the (00) specular and the (01) and $(0\bar{1})$ off-specular reflections, indicative of a smooth surface morphology. Additionally, the films have been characterized by X-ray diffraction, X-ray absorption, AFM and TEM as shown in the appendix and in Ref.16.

Optical studies of both the films and the bare substrates between 20 and 298 K were carried out using reflectance in the range from 6 to 85 meV and variable angle spectroscopic ellipsometry (VASE) in the range from 80 meV to 5.5 eV. Near-normal incidence reflectance measurements were performed in a Michelson interferometer (Bruker 66vs). Reflectance of the sample was first measured relative to a gold reference mirror and then normalized by the reflectance of the gold coated sample.[17] El-

TABLE I. Comparison of relevant theoretical and experimental parameters for LNO films on LAO and STO: lattice mismatch, c-axis parameters obtained from x-ray diffraction, Drude plasma frequency and scattering rate obtained from optics data at 298 K and 20 K, and ratio of the electron kinetic energy obtained from optics data and that obtained from LDA calculations (see text for details).

	Lattice mismatch(%)	c-axis (Å) (XRD)	ω_p 298 K (eV)	ω_p 20 K (eV)	$1/\tau(\omega \to 0)$ 298 K (cm^{-1})	$1/\tau(\omega \to 0)$ 20 K (cm^{-1})	K_{exp}/K_{LDA}
$LaNiO_3/LaAlO_3$	-1.2	3.86	1.11	1.29	468	265	0.11
$LaNiO_3/SrTiO_3$	+1.7	3.78	0.93	1.04	505	403	0.08

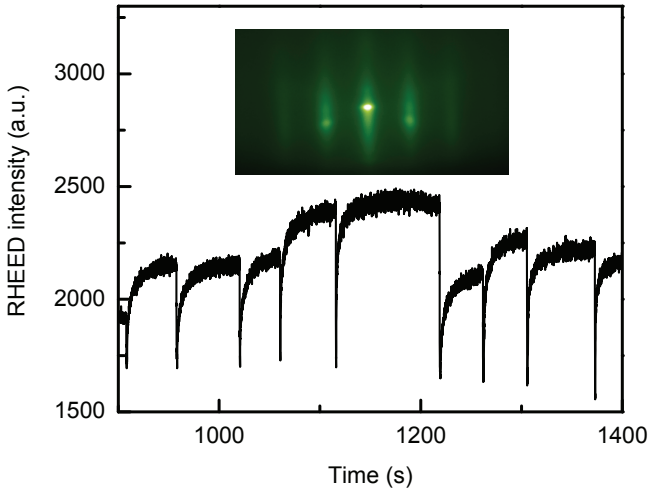

FIG. 1. (color online) Representative RSI evolution during the growth of the LNO film on STO. Inset: corresponding RHEED image.

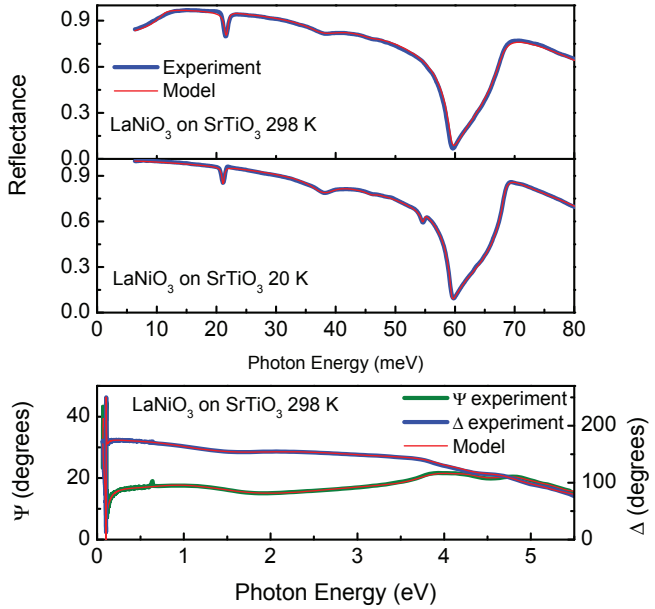

FIG. 2. (color online) Raw reflectance and ellipsometry data for the LNO film on STO plotted with the model fit.

lipsometry measurements were performed with two commercial Woollam ellipsometers. The range from 80 to 550 meV was investigated with an IR-VASE model based on a Bruker 66vs. For the range between 0.6 and 6 eV we used a VASE model based on a grating monochromator. Both ellipsometers are equipped with home-built UHV chambers to allow low temperature measurements.[18] Ellipsometry measurements were performed at incidence angles of 60° and 75°. At each angle, the polarization state of the reflected light was measured in the form of two parameters, Ψ and Δ, which are related to the Fresnel reflection coefficients for p- and s- polarized light ($\tilde{R}_{pp}$ and $\tilde{R}_{ss}$) through the equation

$$\tilde{R} = \frac{\tilde{R}_{pp}}{\tilde{R}_{ss}} = tan(\Psi)e^{i\Delta}. \quad (1)$$

In order to obtain the optical constants from the raw reflectance and ellipsometry data, a model was created using multiple Kramers-Kronig consistent oscillators to describe the complex dielectric function of the sample.[19] The parameters in the model were then fitted to the experimental data using regression analysis with the WVASE32 software package from Woollam Co., Inc. In the case of the LNO films, the model consisted of two layers: a substrate characterized by the optical constants previously determined for either LAO or STO, and a thin film layer from which the optical constants of the film alone were obtained.[19] Since LAO and STO have several far-IR phonons with strong temperature dependence, the substrates were measured and modeled at all the same temperatures as the films. This allows us to use the appropriate temperature for the substrate layer in order to ensure that the temperature dependence observed in the extracted optical conductivity is indeed caused by the LNO films. Representative raw reflectance and ellipsometry data for the film on STO are plotted in Fig.2 along with the model fit.

We note that the crystal structure of the films is slightly anisotropic, with the c-axis lattice parameter about 1.5 % larger (smaller) than the in-plane lattice parameter for the LNO film on LAO (STO). In order to asses the effects of this anisotropy in our optical data, we performed room temperature ellipsometric measurements for the LNO film on LAO in which the position

of the polarizer was varied and tracked. In this way it was possible to obtain the ratios of the diagonal and off-diagonal components of the Jones matrix

$$J = \begin{bmatrix} \tilde{R}_{pp} & \tilde{R}_{sp} \\ \tilde{R}_{sp} & \tilde{R}_{ss} \end{bmatrix}, \quad (2)$$

which is a diagonal matrix when the sample is completely isotropic. We found that the magnitudes of both the real and imaginary parts of $\tilde{R}_{ps}/\tilde{R}_{pp}$ and $\tilde{R}_{sp}/\tilde{R}_{ss}$ were between 0.003 and 0.012 in the the range from 0.6 to 6 eV. This means that the off-diagonal components of the Jones matrix are only about 1% of the diagonal components, approximately the same as the noise level in our measurements. Additionally, modeling using *c*-axis and *ab*-plane optical constants obtained from LDA+DMFT calculations for strained films indicates that our measurements are dominated by the in-plane response and the effect of this anisotropy on the measured ellipsometric parameters is only evident above ∼1.5 eV and is very small. We therefore conclude that the anisotropy of the crystal structure only minimally affects our measurements and the use of an isotropic model for our analysis is appropriate.

Charge self-consistent LDA+DMFT[20] calculations were performed using the implementation described in Ref. 21. We used U=7.3 eV and J=1 eV for the strength of the Coulomb repulsion on Ni-d orbitals, and $E_{DC} = U * (n_d - 1/2) - J(n_d - 1)/2$ as the standard double counting energy, where n_d=7.3 is the average d valence. A range for J and U was determined based on previous studies of this class of compounds and then scanned to obtain the best fit to our optics data as well as to ARPES[22] and thermal measurements.[23] In order to compute the optical conductivity, we analytically continued the self-energy using modified Gaussians[21] and cross-checked the result with maximum entropy. The conductivity was then computed using the DFT momentum matrix elements and convolving the correlated Green's function for all values between -6 eV and 6 eV, relative to the Fermi level.

III. RESULTS AND DISCUSSION

A. Optical conductivity: general trends

Figure 3 shows the real part of the optical conductivity, given by $\sigma(\omega) = \frac{i\omega[1-\epsilon(\omega)]}{4\pi}$, for the LNO films on LAO and STO at various temperatures. In both films, a Drude peak typical of metals is evident at low frequencies, along with three phonon modes. Additionally, four peaks (A-D in Fig.3) can be clearly identified at higher energies. These can be assigned to interband transitions by comparing to LDA theory. The inset in Fig.3 shows a sketch of the LNO density of states (DOS) based on LDA calculations,[13,24–26] indicating a $t_{2g}^6 e_g^1$ electronic configuration, with the antibonding e^*_g states crossing the Fermi level. Figure 4 shows $\sigma_1(\omega)$ of the film on LAO at 100 K along with those obtained from LDA and from LDA+DMFT. The latter was calculated for strained LNO on LAO at 116 K. Using transition decomposition analysis of the LDA optical conductivity we arrive at the assignment of interband transitions reported in Table II.

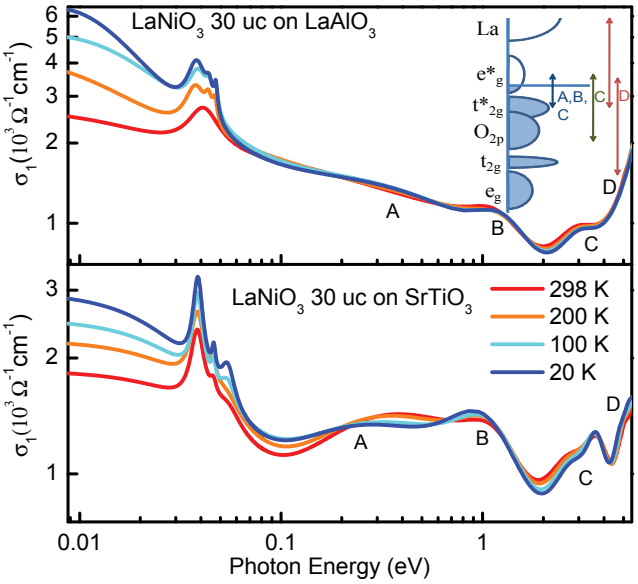

FIG. 3. (color online) Real part of the optical conductivity of fully strained LNO films on LAO (top panel) and STO (botton panel) substrates plotted on a log-log scale. Inset: sketch of the LNO density of states and interband transitions based on LDA calculations.

TABLE II. Assignment of interband transitions based on LDA transition decomposition analysis.

A and B	C	D
$e^*_g \rightarrow e^*_g$	$t^*_{2g} \rightarrow e^*_g$	Ni $3d \rightarrow$ Ni $3d^*$
$t^*_{2g} \rightarrow e^*_g$	O $2p \rightarrow e^*_g$	Ni $3d^* \rightarrow$ La $4f$
		Ni $3d^* \rightarrow$ La $5d$

According to Fig.4, LDA+DMFT provides a more accurate description of our experimental data than LDA does. In particular, feature A is not evident in the LDA $\sigma_1(\omega)$ but is present in the LDA+DMFT results. The two peaks seen at 1 eV and 1.5 eV (A and B, respectively) in LDA shift to lower energy when correlations are included in LDA+DMFT, resulting in better agreement with experiment. In this picture, feature A is due to interband transitions from the t^*_{2g} and e^*_g orbitals. A redshift of feature C is also evident in LDA+DMFT, consistent with the scenario in which electronic correlations suppress the energy of interband transitions due to the quasiparticle renormalization. We note that, even though

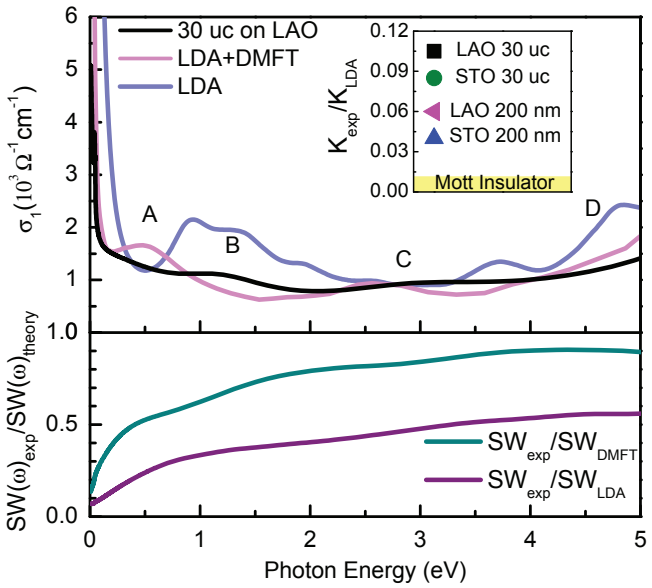

FIG. 4. (color online) Top panel: Real part of the optical conductivity of a 30 unit cell thick LNO film on LAO substrate obtained at 100 K, plotted with the optical conductivity obtained from LDA and LDA+DMFT calculations for strained LNO on LAO at 116 K. Inset: ratio of the experimental electron kinetic energy at room temperature for LNO thin films of different thickness grown on LAO and STO substrates and the LDA kinetic energy. This ratio approaches zero for Mott insulators. Bottom panel: Ratio of the spectral weight obtained from experimental data and that obtained from two different theoretical calculations: LDA and LDA+DMFT.

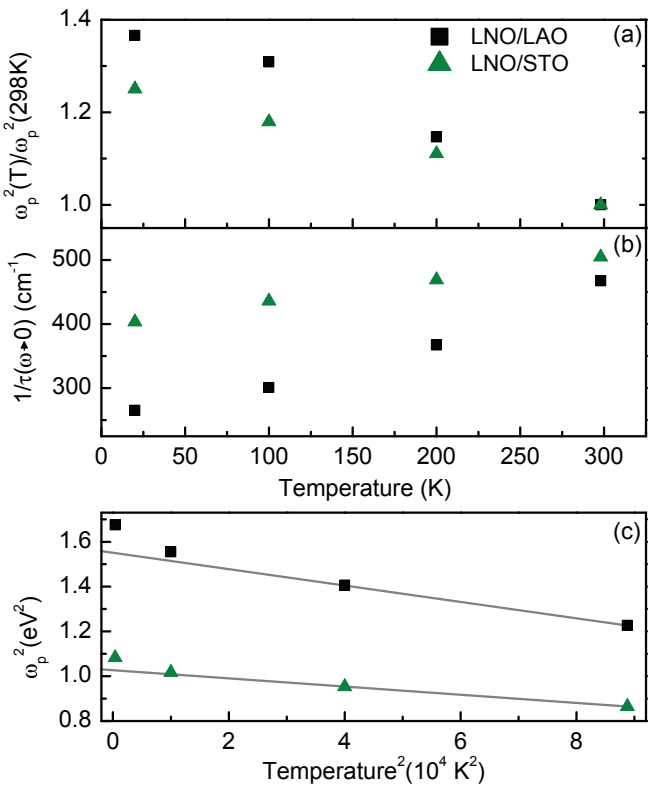

FIG. 5. (color online) (a): Ratio of the Drude plasma frequency at low temperature and at 298 K squared, obtained by integrating the real part of the optical conductivity up to 125 meV. (b): Scattering rate in the zero frequency limit obtained from the extended Drude analysis. (c): Drude plasma frequency squared plotted as a function of the temperature squared.

the LDA+DMFT results reproduce the key experimental trends, the agreement is less than perfect. This is not surprising given that optics is one of the most challenging probes to match well theoretically. This is because the description of the optics data relies on the convolution of two Green's functions, which in turn is very sensitive to any small errors in the individual Green's functions.

B. Extended Drude analysis

In considering the low frequency part of the spectra, it is instructive to first review the usual behavior of the optical conductivity in conventional metals. The free electron (Drude) contribution to the optical conductivity can be described in terms of the electron scattering rate $1/\tau$ using the equation

$$\sigma_{Drude} = \frac{ne^2\tau}{m}\frac{1}{1-i\omega\tau}. \quad (3)$$

In conventional conductors, $1/\tau$ and the carrier mass m are frequency independent and $1/\tau$ decreases with decreasing temperature. This results in an increase in the amplitude and narrowing of the Drude peak. The low and high temperature optical conductivity curves tend to cross before the onset of interband transitions and the Drude plasma frequency remains constant with temperature. The data shown in Fig.3, which are also plotted on a linear scale in the top panels of Fig.6, differ from this description. While the amplitude of the Drude peak increases at low temperature for both films, the narrowing of the Drude peak is not very pronounced, as discussed below.

To understand how our data deviate from the conventional Drude theory, we make use of the extended Drude analysis. Within this framework, the scattering rate $1/\tau(\omega)$ and the mass renormalization factor $m^*(\omega)/m_b$ are understood to be frequency dependent and are given by[6]

$$\frac{1}{\tau(\omega)} = -\frac{\omega_p^2}{\omega} Im\left(\frac{1}{\tilde{\varepsilon}(\omega)-\varepsilon_\infty}\right). \quad (4)$$

$$\frac{m^*(\omega)}{m_b} = -\frac{\omega_p^2}{\omega^2} Re\left(\frac{1}{\tilde{\varepsilon}(\omega)-\varepsilon_\infty}\right). \quad (5)$$

Here m_b is the carrier band mass and ω_p is the Drude

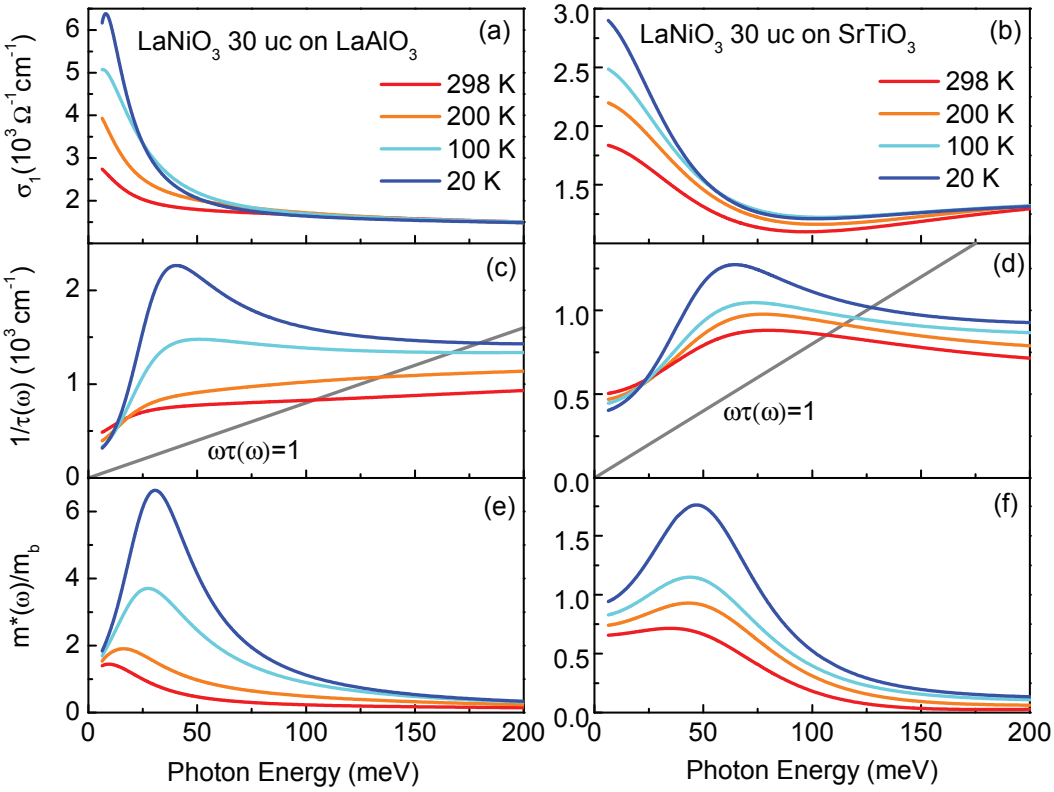

FIG. 6. (color online) Results of the extended Drude analysis for LNO films on LAO (left panels) and on STO (right panels). (a and b): Real part of the optical conductivity after subtraction of the phonon contribution. (c and d): frequency dependent scattering rate. (e and f): frequency dependent mass renormalization factor.

plasma frequency given by

$$\frac{\omega_p^2}{8} = \int_0^{\Omega} \sigma_1 d\omega = \frac{4\pi n e^2}{m}, \qquad (6)$$

with Ω=125 meV. This cut-off was selected to lie between the Drude peak and the onset of interband transitions and provides an upper limit for ω_p. Fig.5 (b) shows $1/\tau(\omega \to 0)$ obtained from Eq. (4). While $1/\tau$ decreases at low temperature, by 20% for the film on STO and by 40% for the film on LAO, the change is not sufficient to account for the increase in DC conductivity. This deficiency is compensated by an increase in the ω_p of up to 20% (Fig.5 (a)), an unusual effect that can be understood as a transfer of spectral weight to the Drude peak and is discussed further in section III C.

Figure 6 shows the results of the extended Drude analysis, along with $\sigma_1(\omega)$ in the same energy range after subtraction of the phonon contribution. As shown in Fig.6(e and f), the mass enhancement is strongly temperature and frequency dependent. $m^*(\omega)/m_b$ increases with decreasing temperature and peaks around 50 meV. We note that $m^*(\omega)/m_b$ is larger for the film on LAO that for the film on STO, especially at low temperature.

As seen in Fig.6(c and d), the low frequency scattering rate of the carriers is larger than their energy ω. This is in contrast with the relation $1/\tau(\omega) < \omega$ characteristic of well defined quasiparticles in a Fermi liquid,[6] and is consistent with the argument for strong electronic correlations in LNO (see section III D). For the film on STO (Fig.6(d)) , $1/\tau(\omega)$ exhibits a peak around 70 meV which increases in magnitude as the temperature is lowered. This type of behavior in $1/\tau(\omega)$ has been attributed to the presence of a pseudogap in other correlated oxides such as underdoped cuprates[27–29] and the metallic puddles in phase separated VO_2.[30] The redshift seen in the peak at low temperature suggests that the magnitude of the gap decreases from 80 meV at 298 K to 65 meV at 20 K. The presence of a pseudogap is also supported by the minimum in the optical conductivity seen in Fig.6(b). For the film on LAO, a peak in $1/\tau(\omega)$ is evident around 40 meV at 20 K and 100 K only (Fig.6(c)), suggesting that a pseudogap develops as the temperatures is lowered. The magnitude of the pseudogap is smaller than for the film on STO and a clear sign of gapping is not apparent in the optical conductivity in Fig.6(a).

C. Temperature dependence

To understand the origin of the anomalous enhancement of the Drude SW, it is useful to look at the ratio of $\sigma_1(\omega)$ at low temperatures and that at 298 K, shown

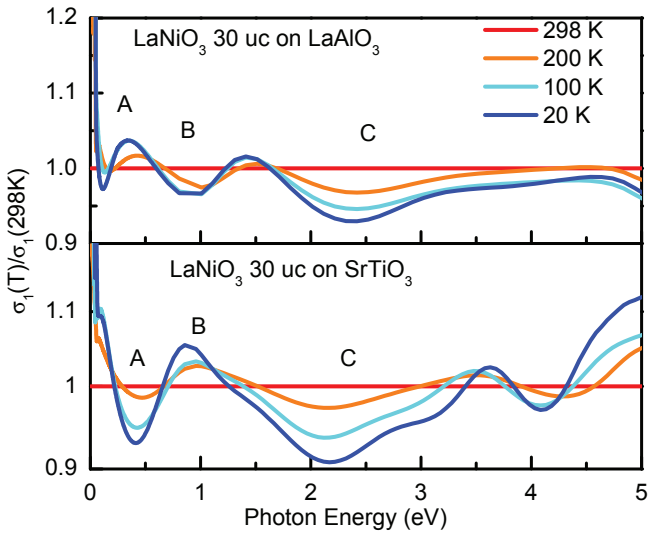

FIG. 7. (color online) Ratio of the optical conductivity at low temperatures and the optical conductivity at 298 K for the LNO films on LAO (top panel) and on STO (bottom panels).

TABLE III. SW of the Drude peak and of feature C at 20 K minus the SW at 298 K for the LNO films on LAO and STO.

	ΔSW_{Drude} (10^5 cm^{-2})	ΔSW_C (10^5 cm^{-2})
LNO/LAO	7.23	-7.15
LNO/STO	3.61	-3.39

in Fig.7. It is apparent from Fig.7 that the temperature dependence of features A and B can be explained as a transfer of SW from one to the other and is opposite in the two films. For the film on LAO (STO), the SW of feature A increases (decreases) and that of feature B decreases (increases) at low temperature. This difference between the two samples could be due to strain, as tensile and compressive strains have been shown to have different effects on the e_g orbitals and DOS in LNO.[16] The reduction in $\sigma_1(\omega)$ between 1.5 and 3.5 eV is more significant and suggests that the enhanced low temperature Drude SW originates from the electronic states responsible for feature C (see Table II). In order to quantify this, we consider the change in SW of the Drude peak ΔSW_{Drude} and of feature C ΔSW_C between 20 K and 298 K, as shown in Table III. The ΔSW_{Drude} and ΔSW_C values are within a few percent of each other for both films, providing strong evidence of SW transfer between feature C and the Drude peak. We note that most of the changes in the Drude part of $\sigma_1(\omega)$ are off the scale in Fig.7 and may be more clearly seen in Fig.5(a). Given U=7.3 eV for LNO, the SW transfer seen in our data appears to be consistent with the canonical half-filled band Hubbard model, in which a SW transfer from the Hubbard band at $U/2$ to the quasiparticle peak is expected.[4] Thus, a similar phenomenology of spectral weight transfer is maintained in LNO despite the fact that the simplest version of the Hubbard band picture needs to be revised for this multiband system with quarter filled e_g bands.

Temperature driven changes in ω_p, along with high energy effects in $\sigma_1(\omega)$, have been observed in several correlated electron systems systems such as high-T_c cuprates,[31,32] manganites[5,7] and V_2O_3.[4] As seen Fig.5(c), the Drude SW plotted as a function of the temperature squared is consistent with a linear behavior. While a T^2/W (where W is the bandwidth) dependence of the SW can be attributed to thermal smearing of the Fermi-Dirac distribution function as given by the Sommerfeld model, these effects are expected to be quite mild in magnitude, unlike the 35% increase in ω_p^2 seen in our data. A T^2 dependence has also been observed in the normal state of high-T_c cuprates,[33–35] in which even changes on the order of 2% are considered to be large based on the bandwidth $W \sim 2$ eV. This deviation from the Sommerfeld model in the cuprates has been attributed to electronic correlations which extend the temperature dependence of the carrier response to energies on the order of U.[35] A direct comparison between the 2-D, single band model in Ref. 35 and our data is not possible since LNO is a multiband, 3-D system. However, given that the e_g bandwidth in LNO is $\sim$ 4 eV, the observed temperature dependence of ω_p is quite substantial and, to our knowledge, unprecedented in the absence of a phase transition.

We note that, since the rest of the lanthanide rare earth nickelates do exhibit an IMT, it is likely that LNO is also close to localization even if it remains metallic at all temperatures. The spectral weight transfer from the low energy Drude peak into the incoherent contribution to the optical conductivity at higher energy is in qualitative agreement with the basic prediction of the DMFT for systems near the Mott transition.[4] Our system specific calculations indeed show that with increasing temperature, the Drude spectral weight gets redistributed to higher energy. However, due to the difficulty associated with the analytic continuation of the Monte Carlo data from the imaginary to the real axis, the precision of the conductivity beyond 1eV is limited, hence we can not determine the theoretical temperature dependence of feature C.

D. Electronic kinetic energy

In earlier work, we reported on the optical properties of LNO films of thickness 100-200 nm, which are expected to be relatively strain free and bulk-like.[13] As in the case of LNO ceramics,[15] no well defined Drude peak was observed in the optical conductivity of these films, presumably due to a combination of enhanced scattering and strong electronic correlations in this material. The fully strained films discussed in this paper and in Ref.12, on the other hand, do exhibit a Drude peak in

the optical conductivity (Fig.3). However, our data show that electronic correlations are still very strong in these films, albeit possibly not as strong as in bulk LNO. In an attempt to quantify and compare the strength of electronic correlations of various LNO films, it is useful to consider the ratio of the electron kinetic energy obtained experimentally and that obtained from band structure calculations K_{exp}/K_{LDA}.[36,37] This ratio is close to unity for conventional metals and becomes suppressed when strong electronic correlations come into play. K_{exp} can be obtained from optical measurements by integrating the Drude contribution of the optical conductivity,[38]

$$K_{exp} = \frac{\hbar c_0}{e^2} \int_0^{\Omega} \frac{2\hbar}{\pi} \sigma_1(\omega) d\omega. \quad (7)$$

Here c_0 is the c-axis lattice parameter and Ω is the frequency cut-off chosen such that interband transitions are excluded from the integral.

The inset in Fig.4 shows K_{exp}/K_{LDA} for various LNO thin film samples at room temperature obtained by integrating $\sigma_1(\omega)$ up to 125 meV, the same cut-off used to obtain ω_p in Fig.5. The same K_{LDA} was used for all the samples. It is clear that K_{exp} is very strongly suppressed with respect to the LDA prediction, regardless of the substrate and thickness of the film. The highest value was obtained for the 30 u.c. film on LAO, K_{exp}/K_{LDA}=0.11, which is very low even compared to other correlated oxides.[37] The data in the inset in Fig.4 suggest that tensile and compressive strain both reduce the strength of correlations in LNO. While it may seem unexpected that both types of strain have a similar effect on the LNO films, we note that the symmetry of the crystal structure is reduced in strained films relative to the bulk, regardless of whether the lattice mismatch is positive or negative. This is due to the epitaxial constraint that removes the 3-fold rotation about the main $R\bar{3}/c$ axis[39] and could be the cause for the increased metallicity of the strained films. Furthermore, it has been shown that the tendency to charge and bond disproportionation is suppressed not only when compressive strain is applied, but also under tensile strain due to the dynamic breathing mode adopted by the oxygen octahedra.[16] Since charge order is the leading cause for the insulating state in nickelates, it can be expected that factors that suppress charge disproportionation will also increase the metallicity of the films. Our data show that this is indeed the case and that the increase in the metallicity is associated with a stronger coherent contribution to the optical conductivity.

The K_{exp}/K_{LDA} values we have obtained are somewhat lower than those reported in Ref.12. Specifically, for a film on LAO they report a mass enhancement of 3 equivalent to $K_{exp}/K_{LDA} = 0.33$, three times higher than our result. Although measurements for a film on STO are not reported, we can estimate from Fig.3 in Ref.12 that an LNO film subject to 1.7% of tensile strain could have mass enhancement of roughly 4, or $K_{exp}/K_{LDA} = 0.25$. This difference is, at least in part, likely due to the choice of integration cut-off Ω. The authors of Ref.12 have chosen $\Omega = 0.2$ eV while in this work we use $\Omega = 0.125$ eV in order to exclude the spectral weight of feature A. Because of the scale on which the optical conductivity is shown in Ref.12 it is hard to assess whether such a feature is present in their data.

While K_{exp}/K_{LDA} depends on the selection of Ω (Eq.(7)), it is important to note that the argument for strong electronic correlations in LNO holds regardless of what cut-off is chosen. The bottom panel in Fig.4 shows the ratio of the spectral weight $SW(\omega) = \int_0^{\omega} \sigma(\omega')d\omega'$ obtained from experimental data and that obtained from LDA calculations. $SW(\omega)$ represents the effective number of carriers contributing to absorption at a given frequency and $SW(\Omega)$ is proportional to K_{exp}. While $SW(\omega)_{exp}/SW(\omega)_{LDA}$ increases with increasing frequency, it remains less than unity over the entire energy range. This shows that, independent of the cut-off frequency used to obtain K_{exp}, LNO is very strongly correlated. The other curve in the bottom panel of Fig.4 shows the spectral weight ratio using LDA+DMFT instead of LDA. Including electronic correlations in the theoretical calculations provides a more realistic description of LNO, resulting in a spectral weight ratio that is closer to unity.

E. Tensile vs. compressive strain

We now compare the effects of tensile and compressive strain on the optical and electronic properties of the LNO films and discuss the findings (see also Table I). Even though the symmetry of the crystal structure in both LNO strained films is reduced relative to the bulk, the films on LAO and STO adopt different lower symmetry space groups ($C2/c$ and $P2_1/c$ respectively).[16,39] For this reason, some differences in the optical response of the two films can be expected. As shown in Figs.3 and 6 the film on LAO has higher $\sigma_1(\omega \to 0)$ than the film on STO. According to Eqs.(3) and (6), the DC conductivity is inversely proportional to $1/\tau$ and proportional to ω_p^2. As seen in Fig.5(b), $1/\tau$ is higher for the film on STO than for the film on LAO. However, this difference is not sufficient to account for the decreased DC conductivity. At 298 K, $\tau_{LAO}/\tau_{STO} = 1.07$ while $\rho_{STO}/\rho_{LAO} = 1.3$. This means that an increased Drude spectral weight for the film on LAO must be included to account for the difference in the conductivity (Fig.5(a)). While $1/\tau$ decreases more rapidly for the film on LAO with decreasing temperature, ω_p remains higher at all temperatures, suggesting that the increased scattering and the reduced Drude spectral weight are jointly responsible for the lower conductivity of the film on STO.

In the context of electronic correlations, the higher ω_p observed for the film on LAO (Fig.5 (a)) means that K_{exp}/K_{LDA} is larger for the film on LAO than for the film on STO (see inset in Fig.4), i.e. the film subject to tensile strain is more strongly correlated than the film

with compressive strain. Furthermore, features B and C are centered at lower frequency for the film on STO than the one on LAO. This is consistent with the hypothesis that electronic correlations suppress the energy of interband transitions (Section III A), as these would be redshifted more in the film with stronger correlations, the film on STO. Our finding is in agreement with X-ray linear dichroism data showing that compressive strain suppresses the tendency to charge and bond disproportionation more so than tensile strain,[16] which could increase the coherent response of the carriers for the film on LAO. Finally, our results are also consistent with the data in Ref.12 showing a larger mass enhancement for the films subject to tensile strain than to compressive strain.

IV. CONCLUSIONS

Our optical study of strained LNO films reveals that, despite the improved metallicity observed in these samples relative to the bulk, three canonical properties of correlated systems are retained: i) a suppression in the ratio K_{exp}/K_{LDA}, ii) a pseudogap and iii) a striking increase in ω_p at low temperature. This latter effect is particularly relevant for the understanding of correlated electron systems, as SW changes of this magnitude have not been previously observed in a correlated system without a phase transition. This result indicates that the low temperature enhancement of the Drude SW can be considered an intrinsic property brought on by electronic correlations, showing that ω_p can be tuned with temperature even in the absence of an IMT.

Finally, we briefly discuss our results in the context of the recent theoretical proposal to mimic the gross features of the cuprate d-bands in nickelates through heterostructuring.[40] Some similarities can be found between LNO and the high-T_c cuprates based on our data. As described above, the temperature dependence of the Drude spectral weight is linear with T^2 (Fig.5(c)). This behavior is consistent with that observed in the normal state of several cuprate superconductors.[33–35] Additionally, features A-C present in the optical conductivity (Fig.3) are also seen in the cuprates.[41] Furthermore, even though our results show an increased metallicity of the strained films relative to bulk LNO, the strength of electronic correlations, possibly a key ingredient for superconductivity,[37] remains quite high. Reference 40 suggests that the presence of tensile strain will be beneficial in the attempt to induce superconductivity in LNO heterostructures. While our data show that strain increases the metallicity of the films, it is the film subject to compressive strain that has the highest conductivity. Therefore, it can not be concluded from our data that tensile strain is more favorable that compressive strain.

V. ACKNOWLEDGMENTS

J.C. was supported by DOD-ARO under grant No. 0402-17291 and NSF grant No. DMR-0747808.

VI. APPENDIX: SAMPLE CHARACTERIZATION

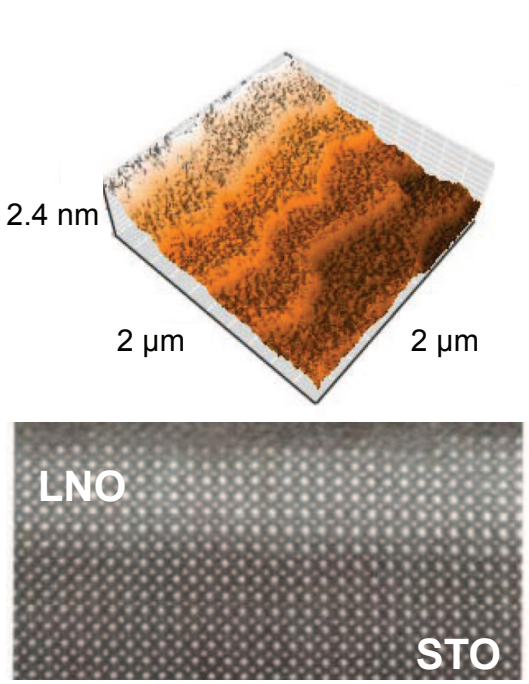

FIG. 8. (color online) Top: AFM surface image of a 30 uc film of LNO on STO. Bottom: TEM image of a 10 uc film of LNO on STO.

In addition to the RHEED measurements shown in Fig.1, the samples have been fully characterized using a variety of techniques to ensure the high quality of the films. The top panel of Fig.8 shows a 2 μm x 2 μm AFM image of a 30 uc LNO film on TiO_2-terminated STO.[42] The image indicates that the sample surface is atomically flat with surface roughness less than 75 pm and preserved vicinal steps. High-resolution cross-sectional TEM imaging (bottom panel of Fig.8) shows a coherent, defect-free film structure and an atomically sharp interface with no cation interdiffusion. Reciprocal space maps of the LNO (222) reflections obtained with X-ray diffraction for 10 uc LNO films on LAO and on STO can be seen in Fig.9. The in-plane components are perfectly matched with respect to the substrates, confirming the fully strained state of the films.

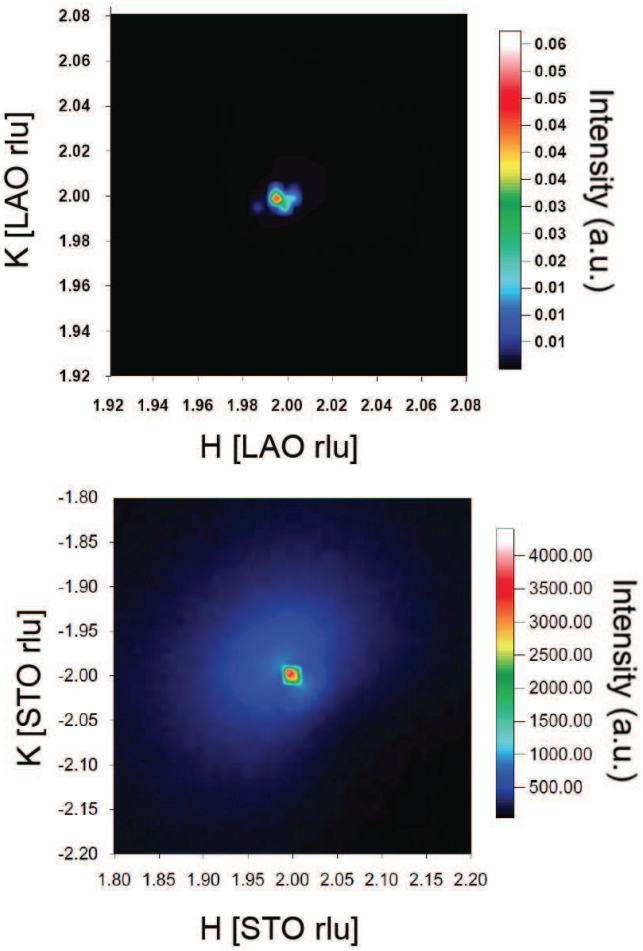

FIG. 9. (color online) Reciprocal lattice maps for 10 uc films of LNO on LAO (top) and on STO (bottom).

* mstewart@physics.ucsd.edu

[1] A. J. Millis and S. N. Coppersmith, Phys. Rev. B **42**, 10807 (1990).
[2] L. Benfatto, J. P. Carbotte, and F. Marsiglio, Phys. Rev. B **74**, 155115 (2006).
[3] D. N. Basov, R. D. Averitt, D. van der Marel, M. Dressel, and K. Haule, Rev. Mod. Phys., accepted for publication.
[4] M. J. Rozenberg, G. Kotliar, H. Kajueter, G. A. Thomas, D. H. Rapkine, J. M. Honig, and P. Metcalf, Phys. Rev. Lett. **75**, 105 (1995).
[5] N. N. Kovaleva, A. V. Boris, C. Bernhard, A. Kulakov, A. Pimenov, A. M. Balbashov, G. Khaliullin, and B. Keimer, Phys. Rev. Lett. **93**, 147204 (2004).
[6] D. N. Basov and T. Timusk, Rev. Mod. Phys. **77**, 721 (2005).
[7] A. Rusydi, R. Rauer, G. Neuber, M. Bastjan, I. Mahns, S. Muller, P. Saichu, B. Schulz, S. G. Singer, A. I. Lichtenstein, et al., Phys. Rev. B **78**, 125110 (2008).
[8] L. Baldassarre, A. Perucchi, D. Nicoletti, A. Toschi, G. Sangiovanni, K. Held, M. Capone, M. Ortolani, L. Malavasi, M. Marsi, et al., Phys. Rev. B **77**, 113107 (2008).
[9] M. M. Qazilbash, A. A. Schafgans, K. S. Burch, S. J. Yun, B. G. Chae, B. J. Kim, H. T. Kim, and D. N. Basov, Phys. Rev. B **77**, 115121 (2008).
[10] K. Sreedhar, J. M. Honig, M. Darwin, M. McElfresh, P. M. Shand, J. Xu, B. C. Crooker, and J. Spalek, Phys. Rev. B **46**, 6382 (1992).
[11] X. Q. Xu, J. L. Peng, Z. Y. Li, H. L. Ju, and R. L. Greene, Phys. Rev. B **48**, 1112 (1993).
[12] D. G. Ouellette, S. B. Lee, J. Son, S. Stemmer, L. Balents, A. J. Millis, and S. J. Allen, Phys. Rev. B **82**, 165112 (2010).
[13] M. K. Stewart, J. Liu, R. K. Smith, B. C. Chapler, C.-H. Yee, K. Haule, J. Chakhalian, and D. N. Basov, arXiv:1005.3314v1 (2010).
[14] J. B. Torrance, P. Lacorre, A. I. Nazzal, E. J. Ansaldo, and C. Niedermayer, Phys. Rev. B **45**, 8209 (1992).
[15] T. Arima, Y. Tokura, and J. B. Torrance, Phys. Rev. B **48**, 17006 (1993).
[16] J. Chakhalian, J. M. Rondinelli, J. Liu, B. Gray, M. Kareev, E. J. Moon, M. Varela, S. G. Altendorf, F. Strigari, B. Dabrowski, et al. (2010).
[17] C. C. Homes, M. Reedyk, D. A. Cradles, and T. Timusk, Appl. Opt. **32**, 2976 (1993).
[18] K. S. Burch, J. Stephens, R. K. Kawakami, D. D. Awschalom, and D. N. Basov, Phys. Rev. B **70**, 205208 (2004).
[19] A. B. Kuzmenko, Rev. Sci. Inst. **76**, 083108 (2005).
[20] G. Kotliar, S. Y. Savrasov, K. Haule, V. S. Oudovenko, O. Parcollet, and C. A. Marianetti, Rev. Mod. Phys. **78**, 865 (2006).
[21] K. Haule, C. H. Yee, and K. Kim, Phys. Rev. B **81**, 195107 (2010).
[22] R. Eguchi, A. Chainani, M. Taguchi, M. Matsunami, Y. Ishida, K. Horiba, Y. Senba, H. Ohashi, and S. Shin, Phys. Rev. B **79**, 115122 (2009).
[23] K. P. Rajeev, G. V. Shivashankar, and A. K. Raychaudhuri, Solid State Commun. **79**, 591 (1991).
[24] D. D. Sarma, N. Shanthi, and P. Mahadevan, J. Phys.: Condens. Matter **6**, 10467 (1994).
[25] I. Solovyev, N. Hamada, and K. Terakura, Phys. Rev.B **53**, 7158 (1996).
[26] Y. Nohara, S. Yamamoto, and T. Fujiwara, Phys. Rev. B **79**, 195110 (2009).
[27] D. N. Basov, R. Liang, B. Dabrowski, D. A. Bonn, W. N. Hardy, and T. Timusk, Phys. Rev. Lett. **77**, 4090 (1996).
[28] A. V. Puchkov, P. Fournier, D. N. Basov, T. Timusk, A. Kapitulnik, and N. N. Kolesnikov, Phys. Rev. Lett. **77**, 3212 (1996).
[29] D. N. Basov, E. J. Singley, and S. V. Dordevic, Phys. Rev. B **65**, 054516 (2002).
[30] M. M. Qazilbash, M. Brehm, G. O. Andreev, A. Frenzel, P. C. Ho, C. Byung-Gyu, K. Bong-Jun, Y. Sun Jin, K. Hyun-Tak, A. V. Balatsky, et al., Phys. Rev. B **79**, 075107 (2009).
[31] D. N. Basov, S. I. Woods, A. S. Katz, E. J. Singley, R. C. Dynes, M. Xu, D. G. Hinks, C. C. Homes, and M. Strongin, Science **283**, 49 (1999).
[32] A. S. Katz, S. I. Woods, E. J. Singley, T. W. Li, M. Xu, D. G. Hinks, R. C. Dynes, and D. N. Basov, Phys. Rev. B **61**, 5930 (2000).
[33] H. J. A. Molegraaf, C. Presura, D. van der Marel, P. H. Kes, and M. Li, Science **295**, 2239 (2002).
[34] G. Deutscher, A. F. Santander-Syro, and N. Bontemps, Phys. Rev. B **72**, 092504 (2005).
[35] M. Ortolani, P. Calvani, and S. Lupi, Phys. Rev. Lett. **94**, 067002 (2005).
[36] A. J. Millis, *Strong Interactions in Low Dimensions* (Kluwer Academic, Dordrecht, The Netherlands, 2004).
[37] M. M. Qazilbash, J. J. Hamlin, R. E. Baumbach, L. J. Zhang, D. J. Singh, M. B. Maple, and D. N. Basov, Nat. Phys. **5**, 647 (2009).
[38] A. J. Millis, A. Zimmers, R. P. S. M. Lobo, N. Bontemps, and C. C. Homes, Phys. Rev. B **72**, 224517 (2005).
[39] S. J. May, J. W. Kim, J. M. Rondinelli, E. Karapetrova, N. A. Spaldin, A. Bhattacharya, and P. J. Ryan, Phys. Rev. B **82**, 014110 (2010).
[40] P. Hansmann, X. P. Yang, A. Toschi, G. Khaliullin, O. K. Andersen, and K. Held, Phys. Rev. Lett. **103**, 016401 (2009).
[41] S. L. Cooper, D. Reznik, A. Kotz, M. A. Karlow, R. Liu, M. V. Klein, W. C. Lee, J. Giapintzakis, D. M. Ginsberg, B. W. Veal, et al., Phys. Rev. B **47**, 8233 (1993).
[42] M. Kareev, S. Prosandeev, J. Liu, C. Gan, A. Kareev, J. W. Freeland, M. Xiao, and J. Chakhalian, Appl. Phys. Lett. **93**, 061909 (2008).